Original Article

An Appreciation for the Rabbit Ladderlike Modeling of Radiation-induced Lung Injury with High-energy X-Ray

Xiang-Ming Fang[1,2], Chun-Hong Hu[1,3], Xiao-Yun Hu[2], Xuan-Jun Yao[2], Ping-Yan Qian[2], Ju-Ying Zhou[4], Jian Guo[4], Alexander Lerner[5]

[1]Imaging Center, The First Affiliated Hospital of Soochow University, Jiangsu 215006, China
[2]Imaging Center, Wuxi People's Hospital Affiliated to Nanjing Medical University, Jiangsu 214023, China
[3]Collaborative Innovation Center of Radiation Medicine of Jiangsu Higher Education Institutions, Suzhou, Jiangsu 215123, China
[4]Radiotherapy Center, The First Affiliated Hospital of Soochow University, Jiangsu 215006, China
[5]Department of Radiology, LAC+USC Medical Center, University of Southern California, Los Angeles, CA, USA

Abstract

Background: To evaluate the utility of rabbit ladderlike model of radiation-induced lung injury (RILI) for the future investigation of computed tomography perfusion.

Methods: A total of 72 New Zealand rabbits were randomly divided into two groups: 36 rabbits in the test group were administered 25 Gy of single fractionated radiation to the whole lung of unilateral lung; 36 rabbits in the control group were sham-radiated. All rabbits were subsequently sacrificed at 1, 6, 12, 24, 48, 72 h, and 1, 2, 4, 8,1 6, 24 weeks after radiation, and then six specimens were extracted from the upper, middle and lower fields of the bilateral lungs. The pathological changes in these specimens were observed with light and electron microscopy; the expression of tumor necrosis factor-α (TNF-a) and transforming growth factor-β1 (TGF-β_1) in local lung tissue was detected by immunohistochemistry.

Results: (1) Radiation-induced lung injury occurred in all rabbits in the test group. (2) Expression of TNF-a and TGF-β_1 at 1 h and 48 h after radiation, demonstrated a statistically significant difference between the test and control groups (each $P < 0.05$). (3) Evaluation by light microscopy demonstrated statistically significant differences between the two groups in the following parameters (each $P < 0.05$): thickness of alveolar wall, density of pulmonary interstitium area (1 h after radiation), number of fibroblasts and fibrocytes in interstitium (24 h after radiation). The test group metrics also correlated well with the time of postradiation. (4) Evaluation by electron microscopy demonstrated statistically significant differences in the relative amounts of collagen fibers at various time points postradiation in the test group ($P < 0.005$), with no significant differences in the control group ($P > 0.05$). At greater than 48 h postradiation the relative amount of collagen fibers in the test groups significantly differ from the control groups (each $P < 0.05$), correlating well with the time postradiation ($r = 0.99318$).

Conclusions: A consistent and reliable rabbit model of RILI can be generated in gradient using 25 Gy of high-energy X-ray, which can simulate the development and evolution of RILI.

Key words: Radiation-induced Lung Injury; Radiation-induced Fibrosis; Radiation Therapy; Rabbit Model

Introduction

Review of prior literature shows that mice or rats were usually selected for establishing animal models of radiation-induced lung injury (RILI).[1-6] However, the death rate was relatively higher because they had greater sensitivity to the radiation. Therefore, only a few animals were able to survive to the advanced phase of pulmonary fibrosis, that is, late phase of RILI. In addition, the mouse model of RILI is not useful for imaging studies such as computed tomography (CT), magnetic resonance and nuclear medicine examinations due to the small size of the lungs of the mouse.[2,4] In contradistinction, the New Zealand white rabbit is more suitable for such a model, as imaging of the lung tissue by CT and magnetic resonance imaging is more feasible, reliable, and as this animal is only moderately sensitive to radiation. Consequently, New Zealand white rabbits were investigated in this study as a potential RILI model to determine the utility and reliability of this animal model for CT perfusion studies.

Access this article online

Quick Response Code:

Website: www.cmj.org

DOI: 10.4103/0366-6999.158323

Methods

Animal groups and experimental procedures

The animal study protocol was approved by the Animal Welfare Committee of the Center of Nanjing Medical University. Seventy-two healthy adult New Zealand white rabbits (supplied by Experimental Animal Center of

Address for correspondence: Prof. Chun-Hong Hu, Imaging Center, The First Affiliated Hospital of Soochow University, Jiangsu 215006, China
E-Mail: hch5305@163.com

Soochow University), including males and females, from 1.0 to 1.2 years old, weighing about 2.5 kg (2.4–2.6 kg) on average were housed separately with 2–3 animals per cage, without limiting feeding or water intake. The animals were randomly divided into the test group (36 rabbits with 25 Gy of single fractioned radiation to the whole lung of unilateral lung) and the control group (36 rabbits with pseudo-radiation, i.e. no radiation after anesthesia). After administration of radiation, all rabbits were sacrificed (by right intracardiac injection of air embolization) at the following time points: 1, 6, 12, 24, 48, 72 h, and 1, 2, 4, 8, 16, 24 weeks. Based on the above postradiation time points, the animal model at different stage of RILI could be established in gradient in order to observe the pathological manifestations at the different phase. If an animal died prior to designated time point, a different additional animal was used instead. For each sacrificed rabbit, open thoracotomy was performed immediately after the CT examination, and then six specimens were collected from the upper, middle and lower lung fields. Ultimately, each specimen was evaluated with the following methods: (1) Hematoxylin and eosin (H & E) staining for light microscopy; (2) transmission electron microscopy; (3) immunohistochemistry to detect the expression of tumor necrosis factor-α (TNF-α), transforming growth factor-β1 (TGF-β1) and other cytokines in the local lung tissue.

Radiation methods

Rabbits were anesthetized with a saline solution containing 30% ethyl carbamate, injected through an ear vein with the dose of 2.5 ml/kg. After their muscles had relaxed fully, the rabbits were fixed in the dorsal position on a custom-made wooden fixture. After completing whole lung CT scan, the target region was delineated and three-dimensional radiation treatment plan was made (using TPS, Xio type from CMS company) to perform unilateral lung radiation including field design and dose calculation. They were located under simulator guide to determine the detailed radiation field. The ipsilateral supraclavicular area, contralateral chest, and the subxiphoid area were blocked with the lead plate. Using linear accelerator (SIEMENS Primus M, Germany), rabbits were irradiated from anterior to posterior direction with 6 mV high energy X-ray, with the central plane of the lung taken as the central radiation level. A single megadose of unilateral lung radiation was performed with the total dose of 25 Gy and the absorbed dose rate of 2 Gy/min. The source axis distance was 100 cm.

Computed tomography scanning methods

Using 64-slice spiral CT scanner (Siemens SOMATOM Definition, Germany), whole lung high resolution scanning was performed when the animals were under deep sedation, and were immobilized by abdominal band with a simple bracket in order to reduce the respiratory motion artifact. The CT examination protocols included: Tube rotation speed of 0.5 s/rotation, rotation angle of 360°, tube voltage of 120 kV, tube current of 100 mAs, FOV of 160 mm, and reconstruction thickness of 1.0 mm.

Pathological examination and evaluation

The changes of the alveoli, alveolar wall, alveolar septum and interstitial capillary were mainly observed under light microscopy after H & E staining. For each subgroup at the 12 times points after radiation, 10 views were randomly selected under the microscope (×10) to measure the thickness of alveolar wall (straight line distance between the adjacent alveoli), interstitial lung density (ratio of interstitial lung area and vision unit area), alveolar surface density (ratio of alveolar lumen area and vision unit area), and the number of the fibers and fibroblasts. For each subgroup, three specimens of one rabbit collected from the upper, middle and lower lung fields in radiation lung were selected in each control group. Similarly, three specimens of three rabbits were selected in each test group. For pathological examination and analysis, 10 views under light microscopy for each specimen were evaluated and compared between every two subgroups of the control and test group. Hence in the control group, $n = 30$; in the test group, $n = 90$ [Tables 1–3]. These measurements were performed using double-blinded method. The average value of each measurement was calculated.

Tumor necrosis factor-α and TGF-β1 staining for immunohistochemistry was performed using Elivison two-step method, and positive results were evaluated and analyzed using the quantitative image analysis method, with number of positive cells, area of positive staining region, and degree of cytoplasm-positive staining (brown) under light microscope calculated using the automated analysis software. Using double-blinded methodology, two senior pathologists randomly selected 20 high power fields (×20 times) for each slice and calculated the average of quantitative indicators for the intensity of reaction (the ratio of the positive staining region accounted for the total area of lung tissue, multiplied by the intensity of reaction). Subsequently, the final result was calculated as the arithmetical mean value of the measurements made by the two pathologists.

HITACHI H-600 (Hitachi, Japan) transmission electron microscopy (TEM) was used for evaluation and photography: To observe ultrastructural changes of the alveolar wall, capillary endothelial cells and basement membrane. Three senior SEM instructors (double blinded) performed 10 microscopic examinations for each specimen (at 10,000 times power) and measured the relative content of collagen, and average value of three measurements was subsequently calculated.

Statistical analysis

The values for thickness of alveolar wall, interstitial lung density, number of fibers and fibroblasts, the average intensity of immunohistochemical reaction, the relative content of collagen and other data were expressed as "mean ± standard deviation." *t*-test was used for evaluation of the differences between the two groups at the same time point. ANOVA was performed for evaluation of mean discrepancy between the different time points. Two-variable linear correlation

Table 1: Comparison between the thickness of alveolar wall, pulmonary interstitial density and alveolar surface density at different time points after radiation

Time after radiation	Alveolar wall thickness (μm)			Pulmonary interstitial density (%)			Alveolar surface density (%)		
	Control	Test	*t*	Control	Test	*t*	Control	Test	*t*
1 h	11.6 ± 1.4	10.9 ± 2.3	1.570	22.8 ± 9.6	25.3 ± 6.7	1.577	82.4 ± 11.9	78.6 ± 7.7*	2.024
6 h	11.0 ± 2.0	13.6 ± 3.4*	3.960	20.4 ± 4.7	29.6 ± 9.2*	5.243	79.3 ± 7.8	76.7 ± 15.6	0.875
12 h	10.4 ± 1.8	16.8 ± 5.9*	5.837	20.2 ± 3.6	37.1 ± 8.9*	10.105	69.5 ± 18.9	64.4 ± 10.8	1.753
24 h	9.9 ± 1.6	28.1 ± 9.2*	10.752	18.7 ± 7.3	41.3 ± 2.8*	24.587	76.6 ± 9.7	56.8 ± 17.5*	5.891
48 h	12.5 ± 2.7	25.5 ± 15.7*	4.501	25.0 ± 7.5	36.2 ± 13.1*	4.438	78.4 ± 12.0	54.6 ± 17.1*	7.056
72 h	10.9 ± 1.7	40.9 ± 9.7*	16.808	21.6 ± 6.4	45.3 ± 12.6*	9.867	80.2 ± 12.4	55.9 ± 8.5*	11.998
1-week	12.6 ± 2.1	33.4 ± 20.0*	5.670	24.6 ± 6.3	53.4 ± 14.3*	11.774	79.0 ± 7.8	44.1 ± 6.8*	23.452
2 weeks	11.8 ± 3.1	37.3 ± 17.4*	7.985	21.5 ± 8.6	43.4 ± 8.1*	12.629	75.3 ± 18.7	46.4 ± 11.4*	10.107
4 weeks	8.6 ± 2.2	29.5 ± 22.1*	5.157	23.6 ± 5.6	51.3 ± 3.4*	32.419	70.1 ± 13.6	35.0 ± 13.3*	12.448
8 weeks	11.4 ± 1.4	53.7 ± 28.8*	8.018	13.1 ± 6.7	54.1 ± 8.4*	24.262	71.1 ± 18.8	34.9 ± 7.9*	14.837
16 weeks	13.0 ± 4.8	79.0 ± 31.1*	10.537	21.8 ± 5.2	68.5 ± 12.0*	20.633	74.9 ± 15.4	26.7 ± 11.2*	18.490
24 weeks	12.4 ± 1.0	61.7 ± 26.0*	10.354	21.0 ± 9.7	73.9 ± 4.7*	39.782	72.4 ± 7.5	23.8 ± 18.6*	13.907

*Difference was statistically significant between the test and control groups ($P < 0.05$); in each subgroup, Control group: $n = 30$, Test group: $n = 90$.

Table 2: Comparison of expression of TNF-α and TGF-β_1 measured in positive staining cells of the lung tissue in control and test groups (%)

Time	TNF-α			TGF-β_1		
	Control	Test	*t*	Control	Test	*t*
1 h	0.69 ± 0.45	1.83 ± 0.67*	8.677	0.23 ± 0.17	0.19 ± 0.15	1.223
6 h	0.73 ± 0.59	3.19 ± 1.15*	11.212	0.21 ± 0.28	0.25 ± 0.18	0.907
12 h	0.76 ± 0.60	6.91 ± 2.22*	14.953	0.28 ± 0.20	0.26 ± 0.14	0.606
24 h	0.68 ± 0.74	5.54 ± 3.08*	8.538	0.26 ± 0.19	0.20 ± 0.19	1.497
48 h	0.66 ± 0.31	4.06 ± 3.14*	5.904	0.24 ± 0.25	0.30 ± 0.29	1.013
72 h	0.75 ± 0.67	3.76 ± 2.29*	7.080	0.24 ± 0.14	0.41 ± 0.27*	3.297
1-week	0.71 ± 0.48	3.45 ± 3.43*	4.349	0.29 ± 0.32	0.53 ± 0.39*	3.043
2 weeks	0.69 ± 0.42	4.15 ± 2.32*	8.102	0.29 ± 0.15	0.52 ± 0.35*	3.486
4 weeks	0.72 ± 0.56	5.23 ± 3.27*	7.497	0.19 ± 0.21	0.79 ± 0.50*	6.373
8 weeks	0.70 ± 0.69	6.01 ± 2.36*	12.121	0.25 ± 0.36	0.60 ± 0.44*	3.936
16 weeks	0.73 ± 0.70	5.34 ± 4.24*	5.912	0.26 ± 0.23	0.81 ± 0.51*	5.704
24 weeks	0.70 ± 1.13	5.51 ± 3.13*	8.221	0.22 ± 0.32	0.83 ± 0.36*	8.253

*Difference was statistically significant between the test and control group ($P<0.05$); in each subgroup, Control group: $n = 30$, Test group: $n = 90$.
TNF-α: Tumor necrosis factor-α; TGF-β_1: Transforming growth factor β_1.

analysis was performed for correlation between pathological indicators and the time points. Statistical analysis was performed with SAS software (version 8.01, SAS Institute Inc.,North Carolina, USA). $P < 0.05$ was used for the designation of statistically significant difference.

Results

Experimental animal appearance, behavior and weight changes

Of the 72 rabbits used for the RILI model, one from the control group died due to an anesthesia complication, two from the test group died on days 1 and 3 after radiation, and the total mortality for the duration of the experiment was 6.3%. Additional animals were used to substitute for the dead rabbits in the corresponding study groups. In the test group, 2 weeks after radiation, the fur of the animals demonstrated thinning in the radiated field, and 6–8 weeks later, the radiated zone demonstrated near complete loss of fur, persisting in this state up to 24 weeks. The rabbits from the test group became less active and less responsive, with gradual deterioration of their activity and responsiveness. The average body weight showed a downward trend over time after radiation starting at 5–7 weeks, and decreasing to 1.9 kg at 16 weeks. The control group showed no abnormalities in appearance, behavior or weight.

Pathological changes

Gross pathology of the lung specimens

The appearance of the lung tissue from the control group was reddish, satiety, smooth, and soft with clear boundary of each leaf. On the contrary, the pulmonary surface and its section showed sporadic hemorrhagic foci after 2 weeks of postradiation. The color of lung tissue, after 8 weeks, appeared to fade, and the boundaries of leaves became unclear, accompanied by a small amount of light yellow pleural effusion. After 16 weeks, lung tissue volume was significantly reduced, and tissue become pale, hard, with an

unclear boundary and pleural adhesions with moderate to a large amount of opaque pleural effusion.

Changes on conventional pathology with hematoxylin and eosin staining

The morphology and structure of the lung tissue were normal in control group specimens [Figure 1a]. In the test group, all the irradiated lung tissue showed abnormal pathologic findings. At 1–24 h after radiation there was swelling of the capillary endothelial cells, congestion within the vascular lumina, large numbers of blood cells leaking into the pulmonary interstitium, thickening of alveolar progressively increasing with time after radiation, increasing pulmonary interstitial density and decreasing alveolar surface density also showing progression over time. The measurements of the alveolar wall thickness and pulmonary interstitial density demonstrated statistically significant differences between the control and test groups [$P < 0.05$, Table 1 and Figure 1b] at all-time points after radiation, also showing linear correlation with time after radiation ($r = 0.82086$, 0.87181, $P = 0.0011$, 0.0002). Pulmonary interstitial fibroblasts and fibrocytes began to proliferate 24 h after radiation, reaching peak at 2 weeks after radiation. After 24 h postradiation, amount of the interstitial fibroblasts and fibrocytes demonstrated statistically significant differences between control and test groups [$P < 0.05$, Table 3] at all-time points, correlating well with the post radiation time in the test group [$r = 0.71764$, $P = 0.0145$], and without such correlation in the test group [$r = -0.15890$, $P = 0.6218$, Figure 2]. At 1–4 weeks after radiation, capillary endothelial cells became swollen with vacuolization and necrotic exfoliation. The vascular lumina were narrowed accompanied by increased intra-alveolar hemorrhage [Figure 1c]. Alveolar type II cells were shed into the alveolar cavity due to necrosis. Macrophages were significantly increased and were engulfing erythrocytes. At about 8 weeks after radiation, capillary endothelia began to proliferate with a fibroblastic hyperplasia of the vascular wall and perivascular tissues of capillary [Figure 1d]. In the test group, the nonirradiated contra-lateral lung showed no such changes. When compared with the control group, the structures described above showed no significant differences.

Table 3: Comparison of the total number of lung fibroblast cells and fibrocytes between the test group and the control group at different time points after radiation

Time	Control ($\times 10^3$)	Test ($\times 10^3$)	t
1 h	2.43 ± 1.31	2.24 ± 0.95	0.858
6 h	2.20 ± 1.28	2.31 ± 1.45	0.370
12 h	1.91 ± 1.26	2.11 ± 0.83	0.944
24 h	1.84 ± 1.37	2.03 ± 0.53	1.098
48 h	2.06 ± 0.82	3.84 ± 1.52*	6.112
72 h	2.59 ± 0.97	4.64 ± 0.78*	11.947
1-week	2.33 ± 1.15	4.53 ± 1.32*	8.151
2 weeks	2.10 ± 0.94	6.74 ± 0.56*	30.774
4 weeks	2.09 ± 0.80	8.76 ± 1.54*	22.679
8 weeks	1.99 ± 1.21	5.36 ± 1.46*	11.396
16 weeks	2.08 ± 1.38	8.76 ± 1.65*	19.954
24 weeks	2.12 ± 1.67	7.66 ± 2.81*	10.197

*Means the difference was statistically significant between the test and control group ($P < 0.05$); in each subgroup, Control group: $n = 30$, Test group: $n = 90$.

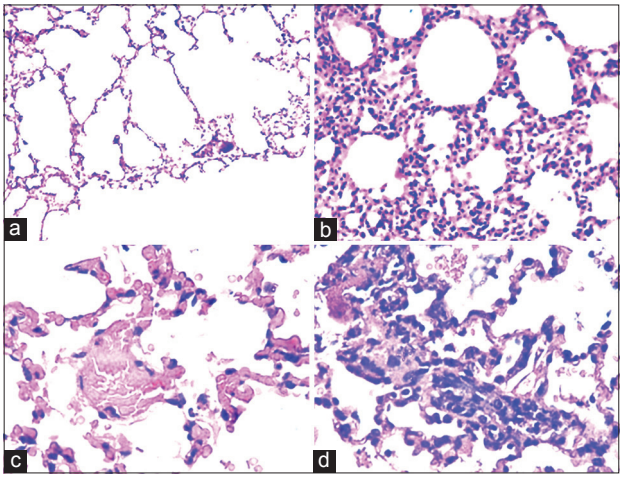

Figure 1: Light microscopy images (H & E, ×40). (a) Lung tissue of control group showed that alveolar wall was thin with regular morphology and normal interstitium; (b) 12 h after radiation of the test group, cells in the alveolar interstitim were significantly increased in number, with focal distribution evolving into a relatively diffuse distribution; (c) 48 h after radiation of the test group, the capillary permeability increased, and a large number of red blood cells leaked into the pulmonary interstitial and into the alveolar space; (d) 8 weeks after radiation of the test group, capillary endothelial cells began to proliferate, and the fibroblast cells proliferated significantly outside of the capillary wall.

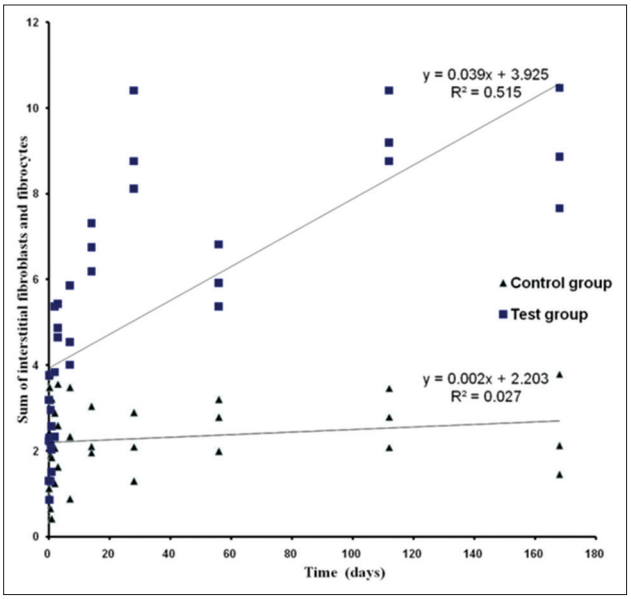

Figure 2: Correlation analysis between pulmonary interstitial fibroblasts and fibrocytes: Block dots represent the test group, with Pearson's related coefficient of $r = 0.68230$, $P = 0.0145 < 0.05$; triangular dots represent the control group, $r = -0.15890$, $P = 0.6218$.

Immunohistochemical analysis

Tumor necrosis factor α expression was significantly enhanced at 1 h after radiation of the lung in the test group (the differences at all-time points were statistically significant in comparison with those of the control group [$P < 0.05$]), and TNF-α expression progressively increased with the prolonged radiation, reaching the maximum value at 12 h ($t = 14.953$, $P < 0.01$). Subsequently expression gradually weakened, and rose again at 4–8 weeks after radiation, and then again decreased gradually by 16 weeks after radiation. TGF-β_1 expression in the test group started to increase gradually at 48 h to 24 weeks after radiation [Figure 3]. The differences were statistically significant at subsequent time points compared to those in the control group [$P < 0.05$, Table 3].

Ultrastructural changes of pulmonary tissue under the electron microscopy

In the control group, the alveolar wall was smooth, with intact morphology of the capillary endothelium and alveolar cells, and with regular and continuous capillary basement membrane. In the test group, there was mild swelling of the mitochondria in Type II alveolar cells, emptying of the lamellar bodies was increased, microvilli were reduced. There was swelling of the capillary endothelial cells at 24 h after radiation with damage of capillary endothelial cells, basement membrane and disruption of the blood barrier starting to become apparent. However, the swelling of the mitochondria of Type II alveolar cells and the emptying of lamellar bodies was more obvious and serious at 48 h after radiation [Figure 4a]. During the same time, Type I alveolar epithelial cells demonstrated vacuolation, with the relative number of collagen fibers beginning to significantly increase in comparison with that of the control group (each $P < 0.05$). These changes correlated well with the radiation time showing a linear correlation ($r = 0.99318$, $P = 0.0$). At 2 weeks to 8 weeks after radiation, electron microscopy revealed vacuolization of Type II epithelial cells, total emptying of lamellar bodies, massive shedding of microvilli, partial necrosis and exfoliation of Type II epithelium, increased vacuolization of capillary endothelial cells, large amount of nondecomposed collagen fibers exudation from the capillaries into the interstitial space and into the alveolar lumen. There was also hyperplasia of Type II alveolar cells, interstitial deposition of fibroblasts and collagen. At 16 weeks to 24 weeks capillary basement membrane was irregularly thickened, Type II alveolar cells were significantly reduced in number, interstitial space and alveolar lumen showed extensive collagen fiber deposition [Figure 4b]. In the test group, the difference in the relative content of the collagen fibers between two radiation time points, was statistically significant ($F = 100.31$, $P = 0$), while in the control group, no such significant difference was found ($F = 1.00$, $P = 0.450$ Table 3).

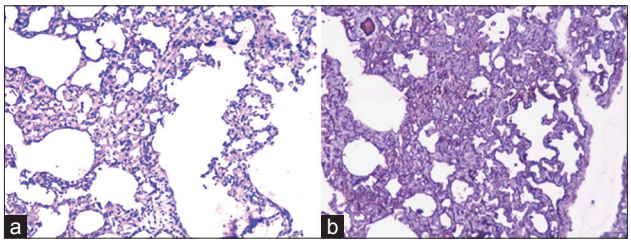

Figure 3: Transforming growth factor β1 (TGF-β1) Immunohistochemistry of the test group (×10). (a) 72 h after radiation, the alveolar wall was moderately thickened, with scattered distribution of positively staining cells with light staining of TGF-β1 positive structures; (b) 8 weeks after radiation, the alveolar wall was significantly thickened with diffuse distribution of positively staining cells with deep staining evident.

Computed tomography findings

At 1 h to 8 weeks after radiation in the test group of rabbits, there were patchy regions of exudation in 16 rabbits [Figure 4c], patchy regions of consolidation changes in 4 rabbits, and ground glass opacities in 8 rabbits. These CT findings were consistent with the early pathological changes of the plasma and inflammatory cells infiltrating lung tissue. At 8–16 weeks, in addition to the above findings, there was lung volume reduction, discrete consolidation, and gradual development of signs of fibrosis, which was consistent with manifestations of intermediate phase of RILI. At 16–24 weeks, exudative and infiltrative lesions almost completely disappeared; however, there was significant fibrosis, solid consolidation and pulmonary atrophy in the partial lung fields consistent with the signs of late phase of RILI [Figure 4d].

Discussion

At present, the diagnosis of RILI depends on imaging findings in combination with appropriate clinical signs and

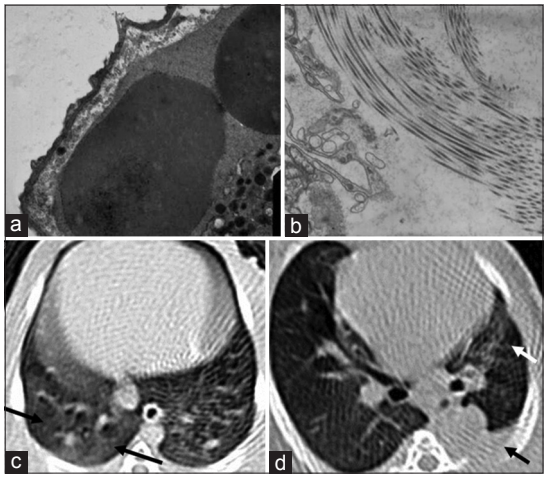

Figure 4: Electron micrograph of the test group specimen (×15000). (a) At 48 h after radiation of the test group, the capillary basement membrane was partly destroyed, and fibrin infiltrated into the pulmonary interstitium; (b) 24 weeks after radiation of the test group, the tissue from the low field of the left lung showed large amount of collagen fibers extensively deposited under the electron microscopy; (c) The computed tomography (CT) image in lung window obtained at 2 weeks showed mild ground-glass opacity in the lower right lung (black arrows); (d) The same model as b, CT image in lung window showed that the left lung volume has decreased with clearly evident scattered areas of fibrosis (white arrow) and left pleural effusion (black arrow).

symptoms. The most objective and accurate diagnostic criteria are based on CT findings.[2,7-9] Unfortunately, when positive findings become apparent on CT imaging, most radiotherapy patients are near the end of their radiotherapy course,[10] so the radiotherapy plan cannot be adjusted and the resultant changes in the lung tissue are difficult to reverse. For this reason, early diagnosis and prediction of RILI is of great clinical value. In our clinical research,[11] we found that CT perfusion, especially pulmonary capillary permeability and other metrics allowed for significantly earlier diagnosis of RILI, as well as improvement in diagnostic accuracy of this entity. Employing a suitable animal model for the study of CT perfusion in early diagnosis and prediction of RILI is crucial for conducting of such investigations.

At this time, research using medium-sized animals for long-term systematic study, such as the rabbit RILI model, is still rare in the literature. Furthermore, animal mortality during administration of the different radiation doses is rarely reported. Based on our preliminary experiments using the rabbit model, RILI could be induced with 25 Gy dose of a single fraction of one whole lung radiation, with the vast majority of animals surviving to the pulmonary fibrosis stage with the overall mortality rate of 6.3%. In the test group, the mortality rate is only 5.6% with only 2 deaths due to the radiation, which indicates that the appropriate dose contributes to the low mortality of rabbit RILI model and the long-term survival after radiation. Based on this investigation, this RILI model can be used for future imaging studies of CT perfusion in this entity.[12]

The RILI pathogenesis has not been fully elucidated at this time. A variety of experiments using the animal model of RILI showed multiple specific characteristics, however the pathologic changes demonstrated similar features in the almost same procedure. Many scholars subcategorize RILI by dividing it into acute and chronic, or early, middle and late phases based on time after radiation.[13] Diffuse alveolar damage associated with interstitial pulmonary congestion, edema, exudation and inflammatory cell infiltration are signs of the pathological changes of the acute phase of RILI. In the chronic phase there is decreased inflammatory cell infiltration, fibroblast proliferation, reduction in the number of capillaries, deformation and atrophy of the alveoli, and extensive interstitial collagen deposition leading to the end stage with disordered fibrous tissue with little inflammation.

Examination with light microscopy showed that focal distribution of inflammatory cell infiltration occurred 1 h after radiation in the test group, and subsequently, these focal lesions progressed, to a diffuse distribution. Meanwhile, exudation of plasma constituents was increasing, the alveolar wall began marked thickening from 12 h to 24 h after radiation, and pulmonary interstitial surface density was correspondingly increasing, and alveolar surface area was gradually decreasing.[3,12,14,15] This phenomenon continued to the end of the experimental time period. Pulmonary capillary endothelial cells, alveolar Type I and II epithelial cells were increasingly impaired along with the time after radiation, which ultimately led to blood barrier derangements.[12,16,17] The increased numbers of interstitial macrophages, fibrocytes, and fibroblasts, demonstrated a linear correlation with time after radiation and were significantly different from those in the control group at each time point more than 24 h after radiation. These results were consistent with those reported in the literature, confirming that this type of model accurately reflects the pathological characteristics in the acute and chronic phases of RILI.[3,15-20]

Examination with electron microscopy in the test group showed that the relative content of the collagen fibers in the radiated lung field had linear correlation with time after radiation, increasing gradually, which provides strong evidence for pulmonary fibrosis in the late phase of RILI. However, collagen and fibrous tissue in this study did not significantly increase until the late phase of RILI. In fact, in the early pathological stage of radiation pneumonia (48 h after radiation), they began increasing (the difference was statistically significant compared with those in control group), and at subsequent time points they continued to increase. At later time points (4–8 weeks) the rate of increase in these metrics became exponential.[20] This phenomenon indicated that radiation pulmonary fibrosis occurred at the same time as radiation induced pulmonary inflammation, rather than following pulmonary inflammation. In other words, radiation pneumonitis and radiation-induced lung fibrosis were neither completely independent of the pathological changes, nor in a completely linear chronological relationship.[11,20] Instead both processes influenced each other with multiple contributing factors including a variety of target cells, cytokines, and free radical damage.[21-23] Hence, based on the above the animal models at different postradiation time points, the meaning and significance of ladderlike model is that the pathological findings at the different stage of RILI are able to be obtained and observed in gradient, simulating the development and evolution of RILI.

The pitfall of this study is that single megadose of unilateral lung radiation was performed with the total dose of 25 Gy without fractions, and this method was likely, not to fully simulate the causes of RILI. However, fractional radiation requires several treatments and a large amount of energy, which was the main deficiency and hardness in the traditional method of RILI modeling. As a result, appreciation was needed for the established model of RILI with a single radiation, which is the main topic for the basic research as well. In fact, this study confirmed that a single radiation with no fractions was able to allow a more efficient methodology for a useful modeling of RILI. CT imaging also showed that the process of RILI was accelerated, so such modeling method could be easily employed and applied to subsequent research of RILI with CT perfusion or other relative researches.[5,11,22]

Radiation-induced lung injury model was successfully implemented using New Zealand white rabbits with unilateral, single high dose radiation methodology. At different time, points after radiation examinations were

performed with light microscopy, electron microscopy and immunohistochemistry showing the same pathological process evolving through multiple stages as reported in the literature. However, each stage of RILI evolution in this model was significantly accelerated, which can lead to time cost savings for a large sample of animals in future research.

References

1. Stelzer KJ, Koh WJ, Peterson LM, Griffin TW. Effect of high-dose pentoxifylline on acute radiation-induced lung toxicity in a rat lung perfusion model. Int J Radiat Oncol Biol Phys 1996;34:111-5.
2. Vujaskovic Z, Down JD, van t' Veld AA, Mooyaart EL, Meertens H, Piers DA, *et al.* Radiological and functional assessment of radiation-induced lung injury in the rat. Exp Lung Res 1998;24:137-48.
3. Pauluhn J, Baumann M, Hirth-Dietrich C, Rosenbruch M. Rat model of lung fibrosis: Comparison of functional, biochemical, and histopathological changes 4 months after single irradiation of the right hemithorax. Toxicology 2001;161:153-63.
4. Ward ER, Hedlund LW, Kurylo WC, Wheeler CT, Cofer GP, Dewhirst MW, *et al.* Proton and hyperpolarized helium magnetic resonance imaging of radiation-induced lung injury in rats. Int J Radiat Oncol Biol Phys 2004;58:1562-9.
5. Sun CY, Zhao YX, Zhong W, Liu DW, Chen YZ, Qin LL, *et al.* The expression of aquaporins 1 and 5 in rat lung after thoracic irradiation. J Radiat Res 2014;55:683-9.
6. Pang QS, Wang P, Wang J, Wang W, Wang J, Yuan ZY. Basic research of the relationship between irradiation dose and volume in radiation-induced pulmonary injury. Chin Med J 2009;122:1929-34.
7. Aoki T, Nagata Y, Negoro Y, Takayama K, Mizowaki T, Kokubo M, *et al.* Evaluation of lung injury after three-dimensional conformal stereotactic radiation therapy for solitary lung tumors: CT appearance. Radiology 2004;230:101-8.
8. Takeda T, Takeda A, Kunieda E, Ishizaka A, Takemasa K, Shimada K, *et al.* Radiation injury after hypofractionated stereotactic radiotherapy for peripheral small lung tumors: Serial changes on CT. AJR Am J Roentgenol 2004;182:1123-8.
9. Larici AR, del Ciello A, Maggi F, Santoro SI, Meduri B, Valentini V, *et al.* Lung abnormalities at multimodality imaging after radiation therapy for non-small cell lung cancer. Radiographics 2011;31:771-89.
10. Przybyszewska M, Miloszewska J, Rzonca S, Trembacz H, Pysniak K, Kotlarz A, *et al.* Soluble TNF-a receptor I encoded on plasmid vector and its application in experimental gene therapy of radiation-induced lung fibrosis. Arch Immunol Ther Exp (Warsz) 2011;59:315-26.
11. Hu XY, Fang XM, Chen HW, Yao XJ, Qian PY, Zhou JY, *et al.* Early detection of acute radiation-induced lung injury with multi-section CT perfusion imaging: An initial experience. Clin Radiol 2014;69:853-60.
12. Kawase T, Kunieda E, Deloar HM, Seki S, Sugawara A, Tsunoo T, *et al.* Experimental stereotactic irradiation of normal rabbit lung: Computed tomographic analysis of radiation injury and the histopathological features. Radiat Med 2007;25:453-61.
13. Marks LB, Yu X, Vujaskovic Z, Small W Jr, Folz R, Anscher MS. Radiation-induced lung injury. Semin Radiat Oncol 2003;13:333-45.
14. Medhora M, Gao F, Fish BL, Jacobs ER, Moulder JE, Szabo A. Dose-modifying factor for captopril for mitigation of radiation injury to normal lung. J Radiat Res 2012;53:633-40.
15. Jackson IL, Vujaskovic Z, Down JD. A further comparison of pathologies after thoracic irradiation among different mouse strains: Finding the best preclinical model for evaluating therapies directed against radiation-induced lung damage. Radiat Res 2011;175:510-8.
16. Takahashi M, Balazs G, Pipman Y, Moskowitz GW, Palestro CJ, Eacobacci T, *et al.* Radiation-induced lung injury using a pig model. Evaluation by high-resolution computed tomography. Invest Radiol 1995;30:79-86.
17. Ao X, Lubman DM, Davis MA, Xing X, Kong FM, Lawrence TS, *et al.* Comparative proteomic analysis of radiation-induced changes in mouse lung: Fibrosis-sensitive and -resistant strains. Radiat Res 2008;169:417-25.
18. Penney DP, Siemann DW, Rubin P, Maltby K. Morphological correlates of fractionated radiation of the mouse lung: Early and late effects. Int J Radiat Oncol Biol Phys 1994;29:789-804.
19. Guerry-Force ML, Perkett EA, Brigham KL, Meyrick B. Early structural changes in sheep lung following thoracic irradiation. Radiat Res 1988;114:138-53.
20. Du ZZ, Ren H, Song JF, Zhang LF, Lin F, Wang HY. Rabbit model of radiation-induced lung injury. Asian Pac J Trop Med 2013;6:237-41.
21. Almeida C, Nagarajan D, Tian J, Leal SW, Wheeler K, Munley M, *et al.* The role of alveolar epithelium in radiation-induced lung injury. PLoS One 2013;8:e53628.
22. Xue J, Li X, Lu Y, Gan L, Zhou L, Wang Y, *et al.* Gene-modified mesenchymal stem cells protect against radiation-induced lung injury. Mol Ther 2013;21:456-65.
23. Bijoux A, Ribou AC. Time-resolved microfluorimetry: An alternative method for free radical and metabolic rate detection in microalgae. Biotechnol J 2014;9:294-300.

Received: 11-01-2015 **Edited by:** De Wang
How to cite this article: Fang XM, Hu CH, Hu XY, Yao XJ, Qian PY, Zhou JY, Guo J, Lerner A. An Appreciation for the Rabbit Ladderlike Modeling of Radiation-induced Lung Injury with High-energy X-Ray. Chin Med J 2015;128:1636-42.

Source of Support: This work was supported by the National Natural Science Foundation of China (NSFC) grants (Youth Fund, No. 81101043), Jiangsu Province Natural Science Foundation (No. BK2011178), the Priority Academic Program Development of Jiangsu Higher Education Institutions (PAPD 2011-0318), and Key Project of Nanjing Medical University Technology Development Fund (No. 2008NMUZ051).
Conflict of Interest: None declared.